DIGITAL ACCESS TO SCHOLARSHIP AT HARVARD
DASH.HARVARD.EDU

HARVARD LIBRARY

Membrane-Assisted Growth of DNA Origami Nanostructure Arrays

Citation

Kocabey, Samet, Susanne Kempter, Jonathan List, Yongzheng Xing, Wooli Bae, Daniel Schiffels, William M. Shih, Friedrich C. Simmel, and Tim Liedl. 2015. "Membrane-Assisted Growth of DNA Origami Nanostructure Arrays." ACS Nano 9 (4): 3530-3539. doi:10.1021/acsnano.5b00161. http://dx.doi.org/10.1021/acsnano.5b00161.

Published version

https://doi.org/10.1021/acsnano.5b00161

Link

http://nrs.harvard.edu/urn-3:HUL.InstRepos:16120984

Terms of use

This article was downloaded from Harvard University's DASH repository, and is made available under the terms and conditions applicable to Other Posted Material (LAA), as set forth at
https://harvardwiki.atlassian.net/wiki/external/NGY5NDE4ZjgzNTc5NDQzMGIzZWZhMGFlOWI2M2EwYTg

Accessibility

https://accessibility.huit.harvard.edu/digital-accessibility-policy

Share Your Story

The Harvard community has made this article openly available.
Please share how this access benefits you. Submit a story

This is an open access article published under an ACS AuthorChoice License, which permits copying and redistribution of the article or any adaptations for non-commercial purposes.

Membrane-Assisted Growth of DNA Origami Nanostructure Arrays

Samet Kocabey,[†] Susanne Kempter,[†] Jonathan List,[‡] Yongzheng Xing,[†] Wooli Bae,[†] Daniel Schiffels,[†] William M. Shih,[§,∥] Friedrich C. Simmel,[‡] and Tim Liedl*,[†]

[†]Fakultät für Physik and Center for Nanoscience, Ludwig-Maximilians-Universität, Geschwister-Scholl-Platz 1, 80539 München, Germany, [‡]Physik-Department, Technische Universität München, Am Coulombwall 4a, 85748 Garching, Germany, and [§]Wyss Institute for Biologically Inspired Engineering and [∥]Biological Chemistry and Molecular Pharmacology, Harvard Medical School, Boston, Massachusetts 02115, United States

ABSTRACT Biological membranes fulfill many important tasks within living organisms. In addition to separating cellular volumes, membranes confine the space available to membrane-associated proteins to two dimensions (2D), which greatly increases their probability to interact with each other and assemble into multiprotein complexes. We here employed two DNA origami structures functionalized with cholesterol moieties as membrane anchors—a three-layered rectangular block and a Y-shaped DNA structure—to mimic membrane-assisted assembly into hierarchical superstructures on supported lipid bilayers and small unilamellar vesicles. As designed, the DNA constructs adhered to the lipid bilayers mediated by the cholesterol anchors and diffused freely in 2D with diffusion coefficients depending on their size and number of cholesterol modifications. Different sets of multimerization oligonucleotides added to bilayer-bound origami block structures induced the growth of either linear polymers or two-dimensional lattices on the membrane. Y-shaped DNA origami structures associated into triskelion homotrimers and further assembled into weakly ordered arrays of hexagons and pentagons, which resembled the geometry of clathrin-coated pits. Our results demonstrate the potential to realize artificial self-assembling systems that mimic the hierarchical formation of polyhedral lattices on cytoplasmic membranes.

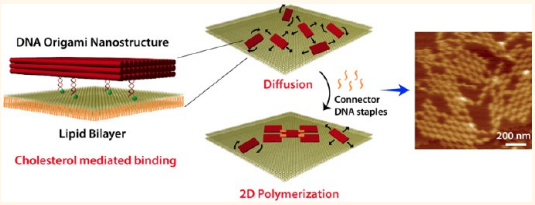

KEYWORDS: DNA origami · DNA nanotechnology · lipid membrane · diffusion · arrays · cholesterol · clathrin

Many of the cellular functions and processes such as trafficking of nutrients, compartmentalization, control of metabolic pathways, immune responses, cell adhesion, and transmembrane charge separation are mediated by the dynamic assembly of membrane-associated protein clusters.[1−3] The proteins clathrin and caveolin, for example, facilitate the formation of intracellular transport vesicles by forming self-assembled complexes upon receptor activation during endocytosis.[4,5] Other transmembrane proteins such as the FAS receptor, which can assemble into the death inducing signal complex, can trigger intracellular signaling pathways upon ligand-activated multimerization.[6,7] All these processes require the orchestrated interaction between various components, which is greatly facilitated through their lateral diffusion and two-dimensional confinement within the lipid membranes of the cells. In a different context, light-induced catalysis of water splitting in plants and bacteria relies on the concerted assembly of many active components into light-harvesting complexes within lipid bilayer membranes.[8,9] In chloroplasts, the membrane between the lumen and stroma fulfills several crucial roles to support efficient photosynthetic charge separation. In addition to the reduction of space and dimensions available to the reactants involved in photosynthesis, it acts as an efficient barrier for charges after they have been pumped across the membrane. Furthermore, it helps to organize the components of the photosynthetic complex with the correct orientation with respect to each other and the surrounding compartments in the first place.

In order to mimic and potentially utilize similar membrane-localized self-assembly mechanisms for nanotechnology applications, we here study the assembly of membrane-bound DNA nanostructures that are inspired by and modeled after membrane-associated protein complexes. DNA nanotechnology allows the construction of arbitrarily shaped objects at the same length scale as protein complexes, which can be

* Address correspondence to tim.liedl@physik.lmu.de.

Received for review January 9, 2015 and accepted March 3, 2015.

Published online March 03, 2015
10.1021/acsnano.5b00161

© 2015 American Chemical Society

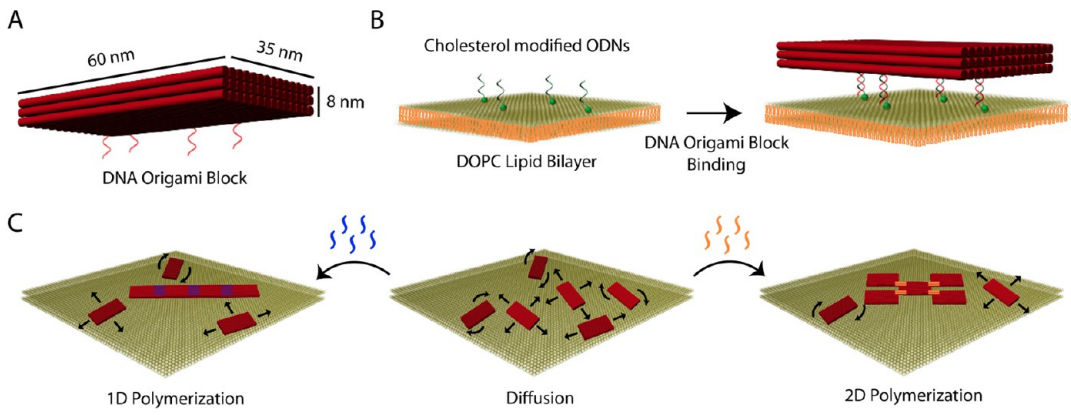

Figure 1. DNA origami block on lipid membrane. (A) DNA origami block structure consisting of three layers of 14 double helices each. The indicated dimensions assume a distance between the base pairs of 0.34 nm and an average distance between the centers of the helices of 2.5 nm. (B) Cholesterol-mediated binding of origami blocks to a lipid bilayer membrane (ODN: oligodeoxynucleotide; DOPC: 1,2-dioleoyl-*sn*-glycero-3-phosphocholine). (C) Programmed polymerization of DNA origami blocks into different superstructures following the addition of connector staples to structures diffusing on the membrane.

easily modified with organic molecules with nanometer precision, defined orientation, and fully controlled stoichiometry. Membrane-encapsulated DNA nanostructures and membrane-spanning DNA nanopores have already been constructed and have been introduced into artificial bilayers by functionalizing these DNA structures with hydrophobic moieties such as cholesterol, ethyl phosphorothioate, or porphyrin.[10−13]

Several characteristics of lipid bilayer membranes are particularly attractive for nanoscale assembly: membranes are extended, quasi two-dimensional structures, which naturally divide space into "cis" and "trans" membrane regions. This confers the possibility to create asymmetric assemblies with different components bound to only one side of a membrane or to embed transmembrane structures in distinct orientations. In addition, the flexibility and fluidity of lipid membranes facilitate the creation of potential nonplanar assemblies, which can change shape or dynamically assemble and disassemble. We here utilize these features to achieve hierarchical organization of DNA nanoobjects into extended superstructures on supported lipid bilayers (SLBs) and on small unilamellar vesicles (SUVs). We characterize the resulting dynamic assemblies by video fluorescence microscopy and high-speed atomic force microscopy (AFM) imaging.

In fact, until now only a few examples of DNA self-assembly across scales have been presented[14−17] even though many fields of research could benefit from large, self-assembled superstructures of molecules ordered in a defined orientation. For example, arrays of optically active subwavelength metamolecules could exhibit novel optical properties,[18] and molecular catalysts inserted into ion-impermeable membranes and assembled with light-funneling nanostructures could be used to create novel photocatalytic systems. Also structural biology could benefit from the arrangement of transmembrane proteins into two-dimensional lattices, which could ultimately be investigated in grazing incident X-ray experiments. Two important steps toward the realization of such applications are the orientation-controlled grafting of molecularly programmable building blocks in and on fluid membranes[19−22] and their subsequent assembly into superstructures of defined geometry.

RESULTS AND DISCUSSION

We built and studied two DNA origami structures: a rectangular, three-layered DNA origami block with dimensions of 60 nm × 35 nm × 8 nm (Figure 1) and a bent DNA origami structure with dimensions of 70 nm × 20 nm × 15 nm that mimics the triskelion assembly of clathrin. Both designs (details can be found in the Supporting Information, Figure S1) allow modification with up to 16 fluorescent dyes and four cholesterol moieties. To this end, we extended staple oligonucleotides with two 18-nt long sequences (anchor sequences), which are complementary to those of a cholesterol-TEG-labeled oligonucleotide and an Alexa488-labeled oligonucleotide (Figure 1A).

We first focus on the block structure in order to illustrate the basic principles of our approach. The three-layered DNA origami block was created as a sufficiently rigid structure that provided multiple positions for functionalization on its top and bottom layer. Structurally rigid building blocks are a necessary prerequisite for the assembly of extended lattices. This was particularly important in the initial phase of the project, when different lattice geometries were explored also in the absence of a supporting substrate. The positions of the cholesterol anchor extensions were chosen such that they were located close to the four edges of the bottom layer of the DNA origami block while the handle sites for the fluorophores were

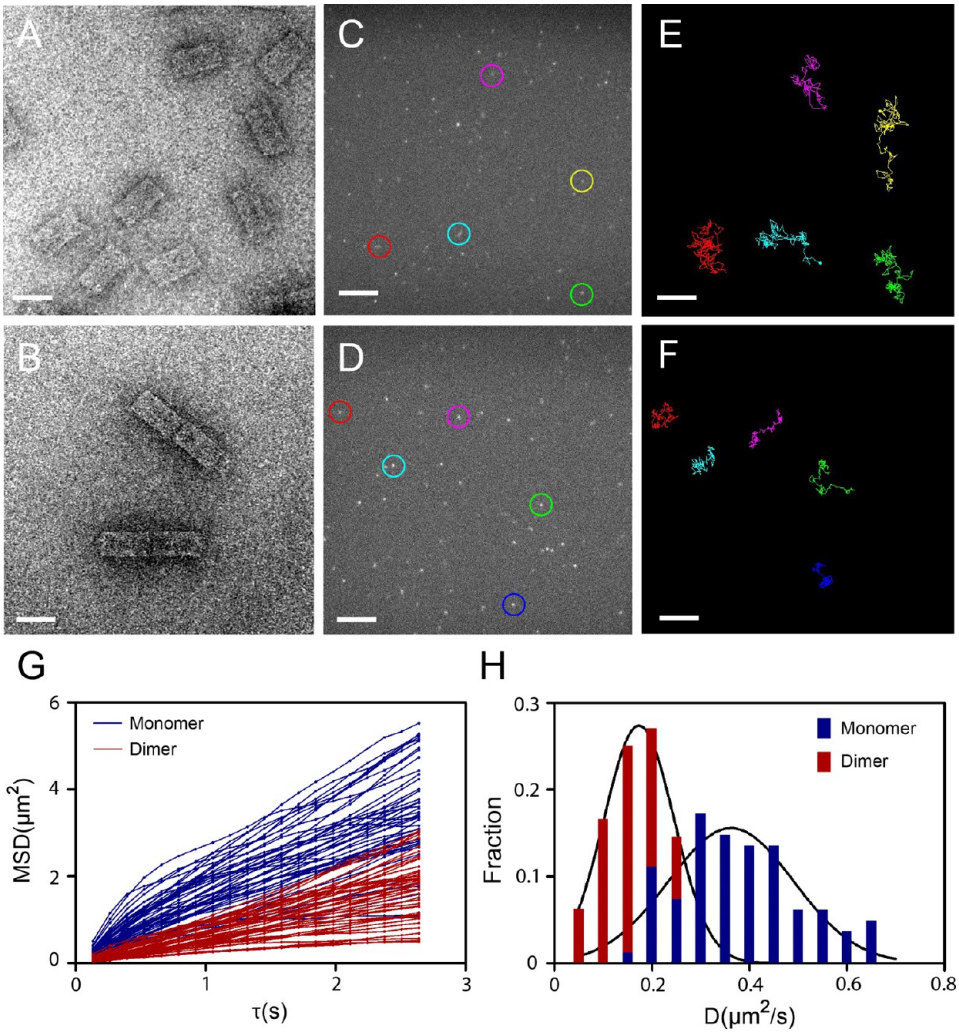

Figure 2. Lateral diffusion of origami block monomers and dimers on supported lipid bilayers. TEM images of DNA origami block monomers (A) and dimers (B) (scale bars: 50 nm). Fluorescence images of DNA origami block monomers (C) and dimers (D) on a DOPC lipid bilayer (scale bars: 5 μm). Example diffusion trajectories for five block monomers (E) and five dimers (F) (scale bars: 5 μm). (G) Time-dependent mean-square displacement (MSD) plot of monomers and dimers. (H) Distribution of diffusion coefficients obtained from single-particle tracking of origami block monomers and dimers. The black lines are Gaussian fits to the distributions.

evenly distributed over the top layer. First, we tested the assembly of DNA origami blocks in the presence of cholesterol-TEG-modified oligonucleotides. Cholesterol-modified structures have a strong tendency to form aggregates in aqueous solutions due to their hydrophobic interactions; in fact, the critical micelle concentration of cholesterol in solution is 25 to 40 nM,[23] which is below the concentration of cholesterol-modified DNA (>100 nM) in our assembly. Agarose gel analysis shows that the origami blocks that were modified with only two cholesterol moieties formed dimers and higher order aggregates (Supporting Information, Figure S2). For this reason, we folded the structures without cholesterol-modified strands and instead incorporated the cholesterol-bearing oligonucleotides into the lipid membrane during formation of the SLB as described below and in Figure 1B. For the sequence-controlled multimerization of the DNA structures we made use of a specific feature of DNA origami designs: single-stranded scaffold loops at the edges of origami structures can be cross-linked by appropriately chosen "multimerization staples", which results in the formation of long chains or structures extended in two dimensions.[14,24−28] In our origami block design we introduced sticky ends to induce end-to-end polymerization in one dimension and a corner-to-corner connection for the formation of a two-dimensional lattice where the nine helices of the front right corner of one block connect to the distant left corner of the next block and *vice versa*, as depicted in Figure 1A and C. DNA origami block dimers were fabricated by fusing two single DNA origami blocks using 12 staple strands as explained in the Supporting Information Figures S3 and S4. Agarose gel analysis and transmission electron microscopy (TEM) revealed the assembly of DNA

origami blocks (Figure 2A and Figure S5) and origami block dimers (Figure 2B and Figure S5) at high yields (93% and 94%, respectively).

To observe grafting of the DNA origami blocks and their subsequent lateral diffusion on artificial lipid membranes by fluorescence microscopy, we prepared lipid bilayers from a 99:1 mixture of 1,2-dioleoyl-*sn*-glycero-3-phosphocholine (DOPC) and 1,1′-dioctadecyl-3,3,3′,3′-tetramethylindodicarbocyanine perchlorate (DiD) inside a microscopy slide flow chamber (Sticky-Slide VI$^{0.4}$, Ibidi; *cf.* Materials and Methods). We then flushed a solution containing the cholesterol-modified oligonucleotides through the channel and incubated it for 1 h. The flow chamber was mounted on an inverted fluorescence microscope to image the membrane and the fluorescently labeled DNA structures that specifically hybridized to the cholesterol-anchored DNA handles. The fluidity of the bilayer was assessed in fluorescence recovery after photobleaching (FRAP) experiments with Texas Red-labeled 1,2-dihexadecanoyl-*sn*-glycero-3-phosphoethanolamine (DHPE) that was introduced at 1% into the membrane (Figure S6). Observation of diffusing DNA origami structures that were specifically attached to the cholesterol handles was crucially dependent on buffer composition. Divalent ions had to be omitted entirely, as the DNA structures stopped diffusing already at low Mg^{2+} concentrations, which we assume is a result of the DNA structures sticking to the glass substrate underneath the bilayer. We thus applied the DNA origami structures (10 pM) to the microscopic chamber in a HEPES buffer (10 mM, pH 7.6) containing only monovalent cations (150 mM NaCl). After 1 h of incubation and several washing steps, we observed adherence and two-dimensional diffusion of DNA origami structures in membranes that were prepared with the cholesterol handles (Figure 2C and D, Supplementary Movies S1 and S2). In control experiments with lipid membranes that lacked such cholesterol handles, in contrast, DNA structures did not adhere and the fluorescent objects moved in and out of the focal plane instead. Membrane-adherent particles were tracked with image analysis software, and 2D diffusion maps were generated as shown in Figure 2E and F. Analysis of single-particle tracks revealed that ~80% of the monomers (n = 748) and dimers (n = 762) were diffusing on the membrane, while the other particles remained stationary. Subdiffraction-sized holes in the membrane may account for the immobile objects, as DNA structures that encounter such a hole will permanently stick to the subjacent substrate.

In order to quantify the diffusive motion of DNA origami block monomers (Figure 2C and E) and dimers (Figure 2D and F) —each modified with either four or eight cholesterol handles—in DOPC lipid membranes, we tracked 84 single particles and 50 dimer particles over time. Examples of particle trajectories obtained from the sequential analysis of 200 frames are presented in Figure 2E and F. From these tracks we extracted the mean square displacement (MSD) of the particles over time using the two-dimensional diffusion equation $\langle \Delta x^2 \rangle = 4D\tau^{\alpha}$. Localization errors were accounted for by applying a confinement offset.[29] The resulting MSD plots displayed in Figure 2G reveal an almost linear increase over time for all tracked particles with a slight tendency for subdiffusional behavior, which may be attributed to occasional defects in the lipid bilayer. We then calculated the diffusion constant of single particles and plotted their relative frequency over D (Figure 2H). The average diffusion coefficients of the DNA origami block monomers were found to be $D_{M,4Chl}$ = 0.4 ± 0.1 $\mu m^2/s$ ($\alpha_{M,\ 4Chl}$ = 0.9 ± 0.1, n = 84) and $D_{M,8Chl}$ = 0.26 ± 0.1 $\mu m^2/s$ ($\alpha_{M,8Chl}$ = 1 ± 0.1, n = 49) for four and eight cholesterol anchors, respectively, while the dimer assemblies yielded $D_{D,4Chl}$ = 0.3 ± 0.1 $\mu m^2/s$ ($\alpha_{D,4Chl}$ = 0.9 ± 0.1, n = 48) and $D_{D,8Chl}$ = 0.2 ± 0.1 $\mu m^2/s$ ($\alpha_{D,8Chl}$ = 1 ± 0.1, n = 50). These values are in reasonable agreement with previous experiments, which were performed using other origami shapes and different experimental conditions. Single-particle tracking of single-layered rectangular DNA origami sheets on SLBs previously resulted in a diffusion coefficient of D = 0.7 $\mu m^2/s$.[18] In fluorescence correlation spectroscopy experiments, DNA origami six-helix bundles were found to diffuse on lipid bilayer vesicles with a larger D = 1.39 $\mu m^2/s$,[19] which may be expected for a membrane in which both lipid layers are fluid.

The standard theoretical model describing the diffusion of objects inside a lipid membrane originally developed by Saffman and Delbrück[30] cannot be directly applied to our experiments, as the DNA structures float on top of the membrane and only a finite number of anchoring cholesterols actually reside within the membrane. On the other hand, the Stokes–Einstein model for objects floating freely in solution predicts diffusion coefficients more than an order of magnitude larger than the observed values. This discrepancy indicates that the drag of the surrounding fluid is negligible and it is indeed the membrane that governs the behavior. Previous studies found that the frictional contributions of few lipid anchors that are coupled but well separated act additively. This is in good agreement with our observation that the measured diffusion constants of DNA structures that carry four cholesterol anchors are almost twice as large as those of the same structures with eight cholesterol anchors.[31,32]

Next, we tested the polymerization of DNA origami blocks on supported lipid bilayers. We used different sets of staples to polymerize DNA origami blocks either into 1D or 2D arrays (*cf.* Figure 1 and Figure S7). Multimerization staples were added to the fluid chamber 1 h after adsorption of the DNA origami blocks on

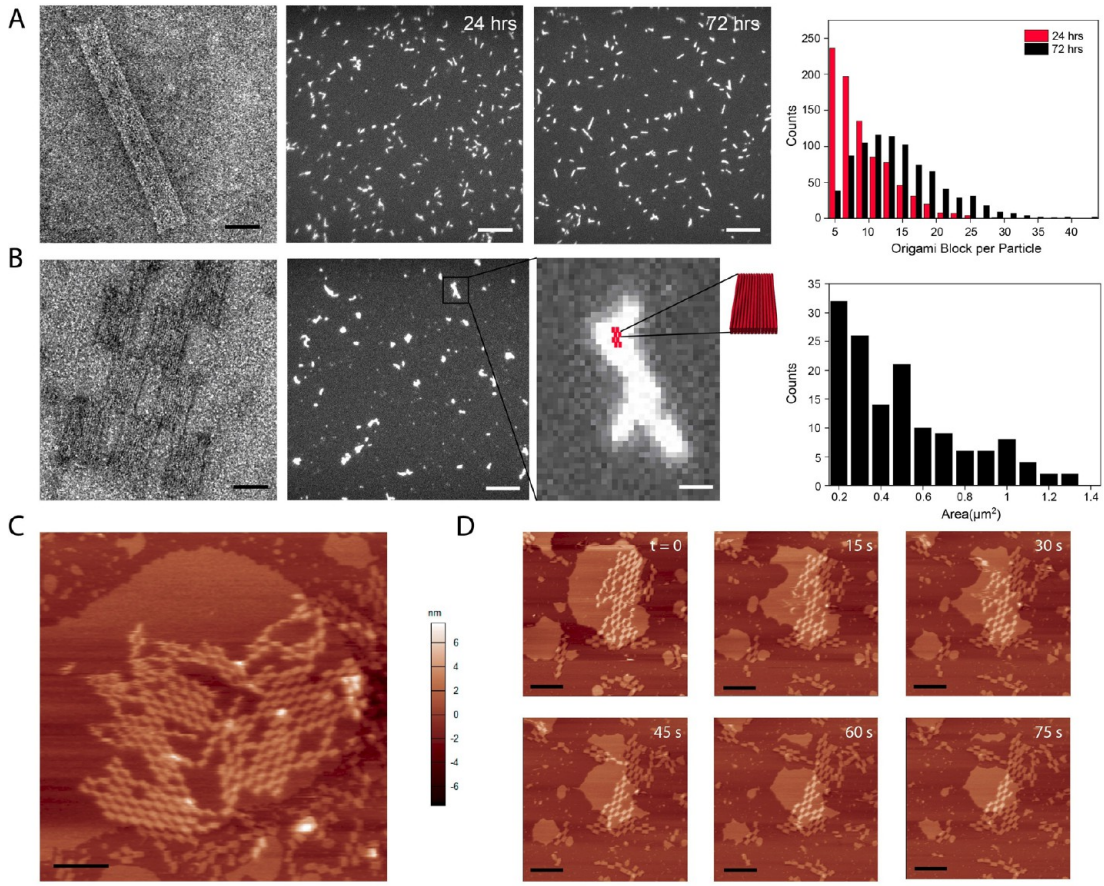

Figure 3. Programmable polymerization of DNA origami blocks on supported lipid bilayers. (A) One-dimensional polymerization. Left: TEM image of polymerized origami blocks after 24 h of incubation in TE buffer with 11 mM Mg^{2+} (scale bar: 50 nm). Middle: Fluorescence images of polymerized origami blocks after 24 and 72 h of incubation on DOPC lipid bilayers (scale bar: 5 μm). Right: Histogram of the estimated number of origami blocks per fluorescent particle after 24 and 72 h of incubation. (B) Two-dimensional polymerization. Left: TEM image of polymerized DNA origami blocks after 24 h of incubation in TE buffer with 11 mM Mg^{2+} (scale bar: 40 nm). Middle: Fluorescence image of polymerized DNA origami blocks after 72 h of incubation (scale bar: 5 μm). Inset: Magnified image of one of the particles including a scheme of a 2D origami lattice for size comparison (scale bar: 400 nm). Right: Histogram of the area of the lattices after 72 h of incubation. (C) AFM image demonstrating lattice formation on the lipid bilayer (scale bar: 300 nm, scan rate: 10 Hz, 512 $\times$ 512 pixels). (D) AFM images showing the decomposition of a lipid bilayer over a time interval of 75 s, which results in the adsorption of an origami lattice on the mica surface (scale bar: 300 nm, scan rate: 10 Hz, 1024 $\times$ 1024 pixels).

the DOPC lipid bilayer and after rigorous washing to flush out monomers that were not yet anchored to the membrane. In fluorescence images taken after 24 and 72 h of incubation time polymers of DNA origami blocks of submicrometer up to 1.5 μm (24 h) and 2.8 μm (72 h) length became visible (Figure 3A). The length distribution would be expected to follow a single exponential for 1D polymerization processes with fixed k_{on} and k_{off} rates if a constant supply of monomers were present in the chambers. Indeed, for the initial phase of the experiment (up to 24 h) we observe an approximately exponential length distribution (Figure 3A). Due to monomer depletion, however, the growth processes stalled and the final length histogram at 72 h deviates from an exponential. Note that we subsumed all particle sizes below the diffraction limit of the fluorescence microscope (~300 nm) into a single histogram bin. It is also noteworthy that we still observed rotational and lateral diffusion of the polymerized DNA origami blocks (Figure S8).

In order to form 2D arrays with the DNA origami blocks we employed a set of staples that pairwise connected the diagonally opposing corners of a block (*cf.* Figure 1 and Figure S9). When the monomer structures were incubated with the multimerization staples without the support of SLBs, TEM images revealed the formation of arrays containing ~10 monomers (Figure 3B). Even the addition of fresh monomers to the solution did not dramatically increase the size of the resulting arrays. In contrast, when the structures were incubated on the SLBs, the fluorescence images showed the formation of extended structures on the micrometer scale (Figure 3B). The area of the largest structure observed corresponds to an assembly of approximately 200 block monomers. High-speed AFM imaging on supported bilayers prepared on mica confirmed our assumptions. For this we

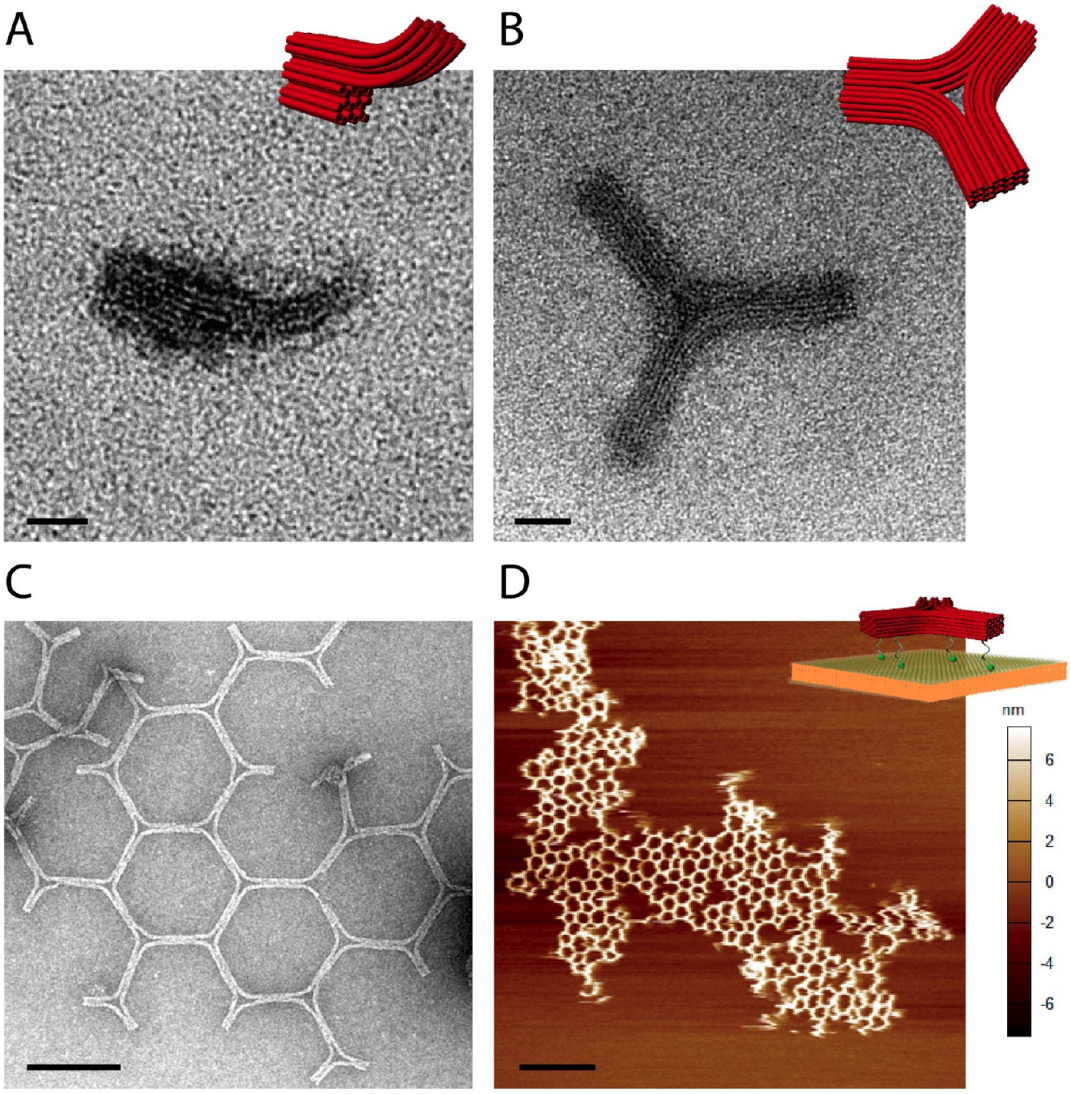

Figure 4. Programmable polymerization of DNA origami triskelions. (A) TEM image of a truncated Y-shaped DNA origami (scale bar: 20 nm). (B) TEM image of a triskelion DNA origami assembled from three truncated Y structures (scale bar: 20 nm). (C) TEM image showing the polymerization of DNA origami triskelions into hexagonal lattices in solution (scale bar: 200 nm). (D) AFM image demonstrating extended polymerization of DNA origami trimers into 2D arrays on supported lipid bilayer (scale bar: 2 μm, scan rate: 4 Hz, 1024 $\times$ 1024 pixels).

prepared lipid bilayers on a mica surface using a solution containing DOPC SUVs in water (*cf.* Materials and Methods). After binding of the DNA origami blocks on the bilayers and overnight incubation, we imaged the samples under various buffer conditions. Imaging in a "low-salt" HEPES buffer containing 150 mM NaCl was not successful, as the origami structures appeared to be too mobile and were pushed around on the bilayer by the AFM cantilever. In order to electrostatically fix the structures on the SLBs, we used an imaging buffer containing high concentrations of $MgCl_2$ (125 mM $MgCl_2$, 400 mM Tris, 200 mM acetic acid, and 10 mM EDTA, pH 8.5), which enabled the observation of DNA block arrays of up to 2 μm in diameter (Figure 3C). Arrays formed in solution, in contrast, were less ordered and far smaller in size (Figure S10). Even at such excessive Mg^{2+} concentrations, DNA nanostructures were still mobile on the mica-supported lipid bilayer during imaging. This resulted in a comparatively low imaging resolution, especially for arrays that were not immobilized at the edges of the bilayer patches. By contrast, DNA arrays touching the underlying mica substrate did not move. As an example, in Figure 3D a time-lapse image series is shown in which a DNA array has initially formed on top of a lipid bilayer. We speculate that due to the high $MgCl_2$ concentration and the repetitive imaging of the same area, the lipid bilayer is partly destroyed and thereby the substrate exposed, this way immobilizing the DNA lattice on the mica surface. At lower $MgCl_2$ concentrations, however, the lipid bilayer stayed intact over several imaging cycles (Figure S11).

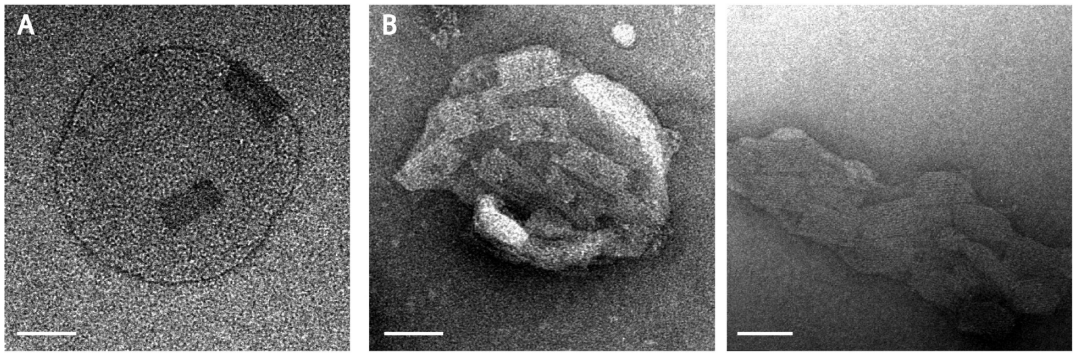

Figure 5. DNA origami block polymerization on SUVs. (A) TEM image of DNA origami block monomers on an SUV (scale bar: 60 nm). (B) 2D lattice formation of the DNA origami blocks on SUVs (scale bars: 60 nm). Interactions between origami lattices and SUVs apparently result in a shape deformation or even destruction of the vesicles.

To further illustrate the potential of our approach to mimic cellular self-assembly processes on artificial lipid bilayer membranes, we designed a second DNA origami structure that is inspired by the protein clathrin.[4] This protein has a three-legged shape (triskelion) and helps to bud off vesicles from the plasma membrane for internalization of molecules that adhered to a cell. The three arms of the triskelion form a 120° angle with respect to each other and furthermore bend slightly out of plane. During membrane budding, the clathrin molecules shape round vesicles by assembling into polyhedral networks consisting of pentagonal and hexagonal rings, the so-called clathrin-coated pits. Our DNA structure has the approximate shape of the letter Y, in which one of the arms has been truncated (Figure 4A). The remaining arm forms a 60° angle[25,33] with the vertical line, and the tip of this arm can be connected with a set of "trimerization" oligonucleotides to the recess of the truncated arm. Three truncated Y's thus form a homotrimer with three legs arranged in 3-fold rotational symmetry (Figure 4B). Upon addition of a set of multimerization oligonucleotides that connect these legs to each other, the homotrimers in turn can assemble into hexagonal arrays (Figure 4C). As the DNA-based structures still have some degree of angular flexibility, also the occasional formation of pentamers can be observed (Figure S12). When we anchored preassembled trimers *via* cholesterol linkers to SLBs on mica and then added the multimerization oligonucleotides, we were able to image arrays consisting of hexamers and pentamers that were several micrometers in diameter (Figure 4D).

Finally, we tested the formation of DNA origami lattices on SUVs in suspension. Following a standard SUV preparation protocol[34] involving tip sonication and extrusion, we obtained SUVs of up to 300 nm in diameter (Figure S13). We first incubated these SUVs with the cholesterol-modified oligonucleotides (HEPES buffer, 150 mM NaCl, pH 7.6) for 15 min, followed by incubation with DNA origami blocks for 1 h. TEM imaging revealed successful binding of DNA origami block monomers to the SUVs (Figure 5A). Subsequent addition of array-forming connector staples led to the formation of 2D array patches on the SUVs. TEM images suggest DNA origami-induced shape deformation of the SUVs, but further studies are required (Figure 5B).

CONCLUSIONS

In this study we explored cholesterol-mediated binding and diffusion of DNA origami structures on supported lipid bilayer membranes and utilized it to create hierarchical assemblies and arrays of such structures with sizes of several micrometers. We found that the measured diffusion coefficients of the individual membrane-anchored DNA structures scale both with the size of the object and with the number of cholesterol anchors that couple the objects to the lipid bilayers, which indicates that the coupled cholesterol moieties are spaced far enough apart to allow free draining of the lipid molecules in between. Importantly, the orientation of the DNA structures with respect to the bilayer is well-defined, as the anchoring is mediated exclusively through DNA anchors that extend from the DNA origami structures on a defined side and couple to cholesterol molecules embedded in the membrane. This predefined orientation of the objects and their confinement to diffuse in 2D allowed the growth of DNA origami arrays that were an order of magnitude larger than those assembled in solution and afterward deposited on a substrate. Arrays of oriented nanostructures tethered to artificial lipid bilayers could be employed to spatially order membrane-associated proteins in their native environment, which could help to study their structural properties with cryo-electron microscopy or X-ray diffraction methods. Moreover, we found that when the arrays were assembled on membranes of small unilamellar vesicles, the binding interactions appeared to be even strong enough to promote the deformation of these SUVs. Our results encourage us to

believe that it will be possible to build DNA objects that mimic biological building blocks such as clathrin or caveolin that play a crucial role in endocytotic processes.

MATERIALS AND METHODS

Preparation of DNA Origami Blocks and Triskelions. All unmodified DNA staple strands (HPSF purified) and dye-modified oligonucleotides (HPLC purified) were purchased from Eurofins MWG Operon (Ebersberg, Germany) (see the Supporting Information, Tables 1 and 2 for sequences) Cholesterol-modified DNA (HPLC purified) was purchased from Biomers (Ulm, Germany). DNA origami structures were designed using caDNAno[35] and prepared by mixing 10 nM M13 based dsDNA scaffold (p8064 for the block structure[36] and p7560 for the origami triskelion) with unmodified staple strands (100 nM each) and 1 μM fluorescently modified staple strands in 1× TE-Mg^{2+} buffer (10 mM Tris-HCl, 1 mM EDTA, 16 mM $MgCl_2$, pH 8.0). In the experiments, between 5 and 16 of the unmodified staple strands were extended at the 3′-end to facilitate hybridization of a fluorescently modified oligonucleotide (5′-Alexa488-GGAAGTTGATATGGTTGATG-3′) to the DNA origami structures. Either four or eight of the unmodified staple strands were extended at the 5′-end to enable hybridization to a cholesterol-modified oligonucleotide (5′-GGTAGTAATAGGAGAATG-CholTEG-3′). The solution was heated to 80 °C for 5 min, cooled to 65 °C over the course of 15 min, and cooled further to 25 °C in 16 h.

Purification and Characterization of DNA Origami Structures. Excess staple strands were removed from DNA origami blocks by agarose gel purification. For this 0.7% agarose was dissolved in 0.5× TBE buffer (pH 8.2) by heating until boiling. $MgCl_2$ (11 mM) was added after cooling, and the solution was poured into a gel cask for solidification. A 200 μL amount of sample solution containing the assembled DNA origami structures and excess staple strands was mixed with 40 μL of 6× loading dye and then loaded into the gel pockets. The gel was run for 2 h at 70 V in an ice-cold water bath to prevent heat-induced denaturation of DNA origami structures. After running, the corresponding band for fluorescently labeled DNA origami structures was cut out from the gel with a razor blade and extracted from the gel by running through spin columns (Freeze'n Squeeze spin columns, Biorad) at 8000*g* for 7 min. The typical concentration of DNA origami structures was 2 nM.

To characterize assembled DNA origami structures, samples were imaged using a JEM-1011 transmission electron microscope (JEOL). DNA origami structures were incubated on argon plasma-exposed (24 W for 1 min) Formvar/carbon-coated grids and then negatively stained with 1% uranyl acetate for 15 s.

Preparation of Lipid Bilayers and DNA Origami Structure Binding. 1,2-Dioleoyl-*sn*-glycero- 3-phosphocholine (Avanti Polar Lipids) and 1,1′-dioctadecyl-3,3,3′,3′-tetramethylindodicarbocyanine perchlorate (Life Technologies) were prepared with 25 and 1 mg/mL concentration in chloroform for supported lipid bilayer formation. DOPC and DiD were mixed at a 99:1 (w/w) ratio in a clean glass vial with a final concentration of 1 mg/mL DOPC. This solution was dried with nitrogen flow for 30 min and further dried in a vacuum oven overnight to make sure any trace chloroform was removed. Dried lipid film was resuspended in 1 mL of PBS buffer (pH 7.4) to obtain a 1 mg/mL lipid suspension. A stock of hydrated lipid suspension was stored at 4 °C for at most 2 weeks.

To prepare supported lipid bilayers, the hydrated lipid suspension stock was diluted to 0.1 mg/mL in 1× PBS buffer. A 100 μL portion of this suspension was injected into the fluidic chamber of a six-channel microscopic slide (Sticky Slide VI$^{0.4}$, Ibidi, Germany) and filled up with 1× PBS buffer. After 1 h incubation of lipid vesicles, the suspension was washed with double-distilled Milli-Q water to induce lipid bilayer formation by osmotic pressure and also to remove excess lipid vesicles. Then, 50 μL of 10 nM cholesterol-TEG-modified oligonucleotide was added to the chamber, and the mixture was incubated for 1 h to embed them into the lipid bilayers. A lipid buffer with monovalent cations (10 mM HEPES, 150 mM NaCl, pH 7.6) was used to dilute cholesterol-modified oligonucleotides and for further washing steps.[22] The stability of the DNA origami structures under these conditions was confirmed using TEM imaging and gel electrophoresis (Figure S14). After incubation for 1 h, unbound oligonucleotides were washed away using lipid buffer. Finally, DNA origami structures were added at a concentration of 10 pM.

Fluorescence Microscopy. Fluorescence images of DNA origami blocks were obtained on a fluorescence microscope (Olympus IX71) equipped with a CCD camera (Hamamatsu ORCA II) using a Olympus PlanApo 100×, 1.4 NA oil immersion objective. Lipid bilayer formation was checked at 647−670 nm (Ex/Em) wavelengths, and DNA origami blocks were visualized at 499−519 nm (Ex/Em) wavelengths.

Fluorescence Recovery after Photobleaching. For FRAP analysis, a DOPC-supported lipid bilayer was prepared as described above, but Texas Red-DHPE was used instead of DiD at the same molar ratio (99:1) for the dye labeling. FRAP was performed with a 532 nm laser (20 mW), and a circular bleach spot with a radius of 6.7 μm surrounding the bleached area was used for data collection and analysis. For the analysis, 20 images were acquired with an interval of 500 ms. The first image captured prior to photobleaching was used to calculate the initial fluorescence intensity followed by 19 consecutive images, in which bleaching and recovery were recorded. FRAP data were further processed using the ImageJ "FRAP Analyzer" plugin. The fluorescence signal was normalized to its respective initial fluorescence intensity prior to photobleaching, and the FRAP curve was constructed using the average fluorescence intensities of the recovery images. Then, the FRAP curve was fitted to a one-phase association fit model with the equation

$$f(t) = a + b \times (1 - e^{-\lambda t})$$

with the fit parameters $a = -0.116$, $b = 0.92$, and $\lambda = 0.2798$/s. To calculate the diffusion coefficient (D) for lateral diffusion of lipids within the lipid bilayer, the "characteristic" diffusion time ($\tau_{1/2} = \ln 2/\lambda$) required to recover 50% of the original fluorescence intensity was calculated from the equation above ($\tau_{1/2} = 2.477$ s) and inserted in the following equation:

$$D = 0.224w^2/\tau_{1/2}$$

where w is the radius of the photobleached spot.[37] The diffusion coefficient (D) of the lipid bilayer was found to be 4.1 μm^2/s.

Single-Particle Tracking and Mean Square Displacement Analysis. DNA origami blocks were added at 10 pM final concentration into a fluidic chamber containing a DOPC SLB. After 1 h of incubation, unbound origami structures were washed away using lipid buffer (10 mM HEPES, 150 mM NaCl, pH 7.6). Lateral diffusion of DNA origami blocks was monitored using mercury lamp excitation. To analyze diffusion, 100 frames from the same spot were acquired with 0.132 s exposure time per frame. At least 20 different fields of view were captured for analysis. Time-averaged mean square displacement analysis was performed using the ImageJ software plugin "Manuel Tracking". Only trajectories of the particles remaining within the frame and which could be tracked for all 100 frames (13.2 s) were analyzed.

To analyze the effect of the DNA origami block size on diffusion, we produced DNA origami block dimers from monomers by connecting them from the same side of two origami block monomers. Twelve connector staples were designed in such a way that half of them could bind to single-strand loops at the edge of one origami block, while the other half could bind to the same edge of another origami block. Each pair of connector staples could hybridize together over a length of 10 nt. Tracking and MSD analysis of block dimers were performed as mentioned above. In total, 81 block monomers and 49 block dimers were analyzed.

1D and 2D Polymerization of Membrane-Bound DNA Origami Blocks. To polymerize DNA origami blocks on DOPC-supported bilayers, DNA origami blocks were added into the fluidic chamber at 10 pM final concentration. After 1 h of incubation, connector staples were added at 100 pM final concentration. 1D polymerization was accomplished using 35 connector staples designed in such a way that every staple could bind to the single-stranded scaffold loop at the other end of the same helix (Figure S7). For 2D polymerization, 16 connector staples were designed to connect opposite corners of the structure by sticky end hybridization (Figure S9). Images were taken by fluorescence microscopy after 24 and 72 h of incubation. The characterization of the DNA block polymers was done using ImageJ software.

AFM Imaging. AFM measurements were performed in tapping mode with an Asylum Research Cypher ES and Olympus BioLever minicantilever (0.1 N/m spring constant) driven at its respective resonance frequency around 18 kHz. A DOPC-supported bilayer was formed on the mica surface by mixing a DOPC/DiD (99:1) solution and distilled water in 1:1 ratio directly after cleavage and incubating for at least 30 min at 37 °C. The sample was washed with distilled water to remove excess vesicles. In order to adsorb DNA nanostructures (500 pM) on the SLB and to facilitate the formation of lattices, the same protocol was applied as for the fluorescence microscopy samples on glass, followed by incubation for at least 12 h. The buffer (10 mM HEPES, 150 mM NaCl, pH 7.6) was then exchanged with a solution containing high concentrations of $MgCl_2$ (125 mM $MgCl_2$, 400 mM Tris, 200 mM acetic acid, and 10 mM EDTA, pH 8.5) to fix the DNA nanostructures to the substrate.

TEM Imaging of SUVs. To visualize DNA origami block polymerization on small unilamellar vesicles, a 1 mg/mL DOPC solution in 10 mM HEPES buffer (150 mM NaCl) was sonicated for 15 min with a tip sonicator. Then, a 0.25 mg/mL SUV suspension was mixed with 100 nM cholesterol-modified DNA in the same buffer. Thirty minutes after incubation, 100 pM DNA origami blocks were added. Finally, connector staples were added at 200 pM final concentration and incubated overnight. Samples were imaged using a JEM-1011 transmission electron microscope (JEOL). DNA origami blocks were incubated on argon plasma-exposed (24 W for 1 min) Formvar/carbon-coated grids and then negatively stained with 1% uranyl acetate for 20 s.

Conflict of Interest: The authors declare no competing financial interest.

Acknowledgment. This work was supported by the European Commission under the Seventh Framework Programme (FP7/2007-2013), as part of the Marie Curie Initial Training Network, EScoDNA (No. 317110) and the ERC grant ORCA, agreement n° 336440, and by the DFG through the SFB 1032 (TPA2 and TPA6) and the Cluster of Excellence Nanosystems Initiative Munich. We thank Prof. Deborah K. Fygenson, Alexander M. Maier, Philip Böhm, and Farzad Sekhavati for their help during DNA origami design, SLB experiments, and data analysis.

Supporting Information Available: Nanostructure design schematics, additional data, and oligonucleotide sequences are available as Supporting Information. This material is available free of charge *via* the Internet at http://pubs.acs.org.

REFERENCES AND NOTES

1. Axelrod, D. Lateral Motion of Membrane Proteins and Biological Function. *J. Membr. Biol.* **1983**, *75*, 1–10.
2. Heldin, C. H. Dimerization of Cell Surface Receptors in Signal Transduction. *Cell* **1995**, *80*, 213–223.
3. Lamb, T. D. Gain and Kinetics of Activation in the G-Protein Cascade of Phototransduction. *Proc. Natl. Acad. Sci. U.S.A.* **1996**, *93*, 566–570.
4. Pearse, B. M. Clathrin: A Unique Protein Associated with Intracellular Transfer of Membrane by Coated Vesicles. *Proc. Natl. Acad. Sci. U.S.A.* **1976**, *73*, 1255–1259.
5. Doherty, G. J.; McMahon, H. T. Mechanisms of Endocytosis. *Annu. Rev. Biochem.* **2009**, *78*, 857–902.
6. Kischkel, F. C.; Hellbardt, S.; Behrmann, I.; Germer, M.; Pawlita, M.; Krammer, P. H.; Peter, M. E. Cytotoxicity-Dependent APO-1 (Fas/CD95)-Associated Proteins Form a Death-Inducing Signaling Complex (DISC) with the Receptor. *EMBO J.* **1995**, *14*, 5579–5588.
7. Ashkenazi, A.; Dixit, V. M. Death Receptors: Signaling and Modulation. *Science* **1998**, *281*, 1305–1308.
8. Deisenhofer, J.; Epp, O.; Miki, K.; Huber, R.; Michel, H. X-ray Structure Analysis of a Membrane Protein Complex. *J. Mol. Biol.* **1984**, *180*, 385–398.
9. Liu, Z.; Yan, H.; Wang, K.; Kuang, T.; Zhang, J.; Gui, L.; An, X.; Chang, W. Crystal Structure of Spinach Major Light-Harvesting Complex at 2.72 A Resolution. *Nature* **2004**, *428*, 287–292.
10. Langecker, M.; Arnaut, V.; Martin, T. G.; List, J.; Renner, S.; Mayer, M.; Dietz, H.; Simmel, F. C. Synthetic Lipid Membrane Channels Formed by Designed DNA Nanostructures. *Science* **2012**, *338*, 932–936.
11. Burns, J. R.; Stulz, E.; Howorka, S. Self-Assembled DNA Nanopores That Span Lipid Bilayers. *Nano Lett.* **2013**, *13*, 2351–2356.
12. Burns, J. R.; Gopfrich, K.; Wood, J. W.; Thacker, V. V.; Stulz, E.; Keyser, U. F.; Howorka, S. Lipid-Bilayer-Spanning DNA Nanopores with a Bifunctional Porphyrin Anchor. *Angew. Chem., Int. Ed.* **2013**, *52*, 12069–12072.
13. Perrault, S. D.; Shih, W. M. Virus-Inspired Membrane Encapsulation of DNA Nanostructures to Achieve *in Vivo* Stability. *ACS Nano* **2014**, *8*, 5132–5140.
14. Zheng, J.; Birktoft, J. J.; Chen, Y.; Wang, T.; Sha, R.; Constantinou, P. E.; Ginell, S. L.; Mao, C.; Seeman, N. C. From Molecular to Macroscopic *via* the Rational Design of a Self-Assembled 3D DNA Crystal. *Nature* **2009**, *461*, 74–77.
15. Liu, W.; Zhong, H.; Wang, R.; Seeman, N. C. Crystalline Two-Dimensional DNA-Origami Arrays. *Angew. Chem., Int. Ed.* **2011**, *50*, 264–267.
16. Schreiber, R.; Do, J.; Roller, E.-M.; Zhang, T.; Schuller, V. J.; Nickels, P. C.; Feldmann, J.; Liedl, T. Hierarchical Assembly of Metal Nanoparticles, Quantum Dots and Organic Dyes Using DNA Origami Scaffolds. *Nat. Nanotechnol.* **2014**, *9*, 74–78.
17. Aghebat Rafat, A.; Pirzer, T.; Scheible, M. B.; Kostina, A.; Simmel, F. C. Surface-Assisted Large-Scale Ordering of DNA Origami Tiles. *Angew. Chem., Int. Ed.* **2014**, *53*, 7665–7668.
18. Zheludev, N. I.; Kivshar, Y. S. From Metamaterials to Metadevices. *Nat. Mater.* **2012**, *11*, 917–924.
19. Suzuki, Y.; Endo, M.; Yang, Y.; Sugiyama, H. Dynamic Assembly/Disassembly Processes of Photoresponsive DNA Origami Nanostructures Directly Visualized on a Lipid Membrane Surface. *J. Am. Chem. Soc.* **2014**, *136*, 1714–1717.
20. List, J.; Weber, M.; Simmel, F. C. Hydrophobic Actuation of a DNA Origami Bilayer Structure. *Angew. Chem., Int. Ed.* **2014**, *53*, 4236–4239.
21. Johnson-Buck, A.; Jiang, S.; Yan, H.; Walter, N. G. DNA-Cholesterol Barges as Programmable Membrane-Exploring Agents. *ACS Nano* **2014**, *8*, 5641–5649.
22. Czogalla, A.; Petrov, E. P.; Kauert, D. J.; Uzunova, V.; Zhang, Y.; Seidel, R.; Schwille, P. Switchable Domain Partitioning and Diffusion of DNA Origami Rods on Membranes. *Faraday Discuss.* **2013**, *161*, 31–43.
23. Haberland, M. E.; Reynolds, J. A. Self-Association of Cholesterol in Aqueous Solution. *Proc. Natl. Acad. Sci. U.S.A.* **1973**, *70*, 2313–2316.
24. Douglas, S. M.; Dietz, H.; Liedl, T.; Hogberg, B.; Graf, F.; Shih, W. M. Self-Assembly of DNA into Nanoscale Three-Dimensional Shapes. *Nature* **2009**, *459*, 414–418.
25. Dietz, H.; Douglas, S. M.; Shih, W. M. *Folding DNA into Twisted and Curved Nanoscale Shapes* **2009**, *325*, 725–730.
26. Rothemund, P. W. Folding DNA to Create Nanoscale Shapes and Patterns. *Nature* **2006**, *440*, 297–302.
27. Jungmann, R.; Scheible, M.; Kuzyk, A.; Pardatscher, G.; Castro, C. E.; Simmel, F. C. DNA Origami-Based Nanoribbons: Assembly, Length Distribution, and Twist. *Nanotechnology* **2011**, *22*, 275301.
28. Woo, S.; Rothemund, P. W. Programmable Molecular Recognition Based on the Geometry of DNA Nanostructures. *Nat. Chem.* **2011**, *3*, 620–627.

29. Wieser, S.; Schutz, G. J. Tracking Single Molecules in the Live Cell Plasma Membrane-Do's and Don't's. *Methods* **2008**, *46*, 131–140.
30. Saffman, P. G.; Delbruck, M. Brownian Motion in Biological Membranes. *Proc. Natl. Acad. Sci. U.S.A.* **1975**, *72*, 3111–3113.
31. Knight, J. D.; Lerner, M. G.; Marcano-Velazquez, J. G.; Pastor, R. W.; Falke, J. J. Single Molecule Diffusion of Membrane-Bound Proteins: Window into Lipid Contacts and Bilayer Dynamics. *Biophys. J.* **2010**, *99*, 2879–2887.
32. Tamm, L. K. Lateral Diffusion and Fluorescence Microscope Studies on a Monoclonal Antibody Specifically Bound to Supported Phospholipid Bilayers. *Biochemistry* **1988**, *27*, 1450–1457.
33. Castro, C. E.; Kilchherr, F.; Kim, D. N.; Shiao, E. L.; Wauer, T.; Wortmann, P.; Bathe, M.; Dietz, H. A Primer to Scaffolded DNA Origami. *Nat. Methods* **2011**, *8*, 221–229.
34. Mingeot-Leclercq, M. P.; Deleu, M.; Brasseur, R.; Dufrene, Y. F. Atomic Force Microscopy of Supported Lipid Bilayers. *Nat. Protoc.* **2008**, *3*, 1654–1659.
35. Douglas, S. M.; Marblestone, A. H.; Teerapittayanon, S.; Vazquez, A.; Church, G. M.; Shih, W. M. Rapid Prototyping of 3D DNA-Origami Shapes with caDNAno. *Nucleic Acids Res.* **2009**, *37*, 5001–5006.
36. Stein, I. H.; Schuller, V.; Bohm, P.; Tinnefeld, P.; Liedl, T. Single-Molecule FRET Ruler Based on Rigid DNA Origami Blocks. *ChemPhysChem* **2011**, *12*, 689–695.
37. Soumpasis, D. M. Theoretical Analysis of Fluorescence Photobleaching Recovery Experiments. *Biophys. J.* **1983**, *41*, 95–97.